Magnesium Technology 2011
Edited by: Wim H. Sillekens, Sean R. Agnew, Neale R. Neelameggham, and Suveen N. Mathaudhu
TMS (The Minerals, Metals & Materials Society), 2011

LOW-CYCLE FATIGUE BEHAVIOR OF DIE-CAST Mg ALLOY AZ91

Luke Rettberg[1], Warwick Anderson[1], J. Wayne Jones[1]

[1]University of Michigan, Gerstacker Building Rm. 1021, 2200 Bonisteel Blvd; Ann Arbor, MI, 48109, USA

Keywords: Low-Cycle Fatigue, Die-Cast AZ91, Strain-Life, Hysteresis Loops, Incremental Step Test, Cyclic Stress-Strain, Microstructure, Fractography, Porosity

Abstract

An investigation has been conducted on the influence of microstructure and artificial aging response (T6) on the low-cycle fatigue behavior of super vacuum die-cast (SVDC) AZ91. Fatigue lifetimes were determined from total strain-controlled fatigue tests for strain amplitudes of 0.2%, 0.4% and 0.6%, under fully reversed loading at a frequency of 5 Hz. Cyclic stress-strain behavior was determined using incremental step test (IST) methods. Two locations in a prototype casting with different thicknesses and, therefore, solidification rates, microstructure and porosity, were examined. In general, at all total strain amplitudes fatigue life was unaffected by microstructure refinement and was attributed to significant levels of porosity. Cyclic softening and a subsequent increased cyclic hardening rate, compared to monotonic tests, were observed, independent of microstructure. These results, fractography and damage accumulation processes, determined from metallographic sectioning, are discussed.

Introduction

In recent years, magnesium alloys have gained renewed interest due to their low density and high specific strength. For automotive applications, reducing weight is important to improve fuel economy. For example, replacing steel and aluminum with magnesium in heavy components could result in a $0.25L$ and $0.1L$ per $100km$ reduction in fuel consumption, respectively [1]. North American automotive manufacturers plan to substitute $340lbs.$ of magnesium components for $630lbs.$ of current ferrous and aluminum parts by 2020 [2].

The ternary Mg-Al-Zn alloy AZ91 has excellent castability, mechanical properties at ambient temperature, corrosion resistance and is the most commonly used magnesium die-casting alloy [3]. However, before AZ91 can be used for structural components in automobiles, fatigue properties must be further characterized. Fatigue properties are relevant for such components where cyclic loading rather then constant stress limits service life [4]. For fatigue modeling, the cyclic stress-strain properties need to be characterized and the impact of heat treatment determined. Some work has already been done in this area [5–9] and the goal of this paper is to further examine the effects of microstructure refinement and aging on the low-cycle fatigue and cyclic stress-strain properties of die-cast AZ91. The influence of microstructure on damage accumulation and crack initiation was also examined.

Experimental Procedure

Fatigue specimens were machined from two locations on a prototype die-cast AZ91 shock tower. The two locations (L1 & L2) had the greatest difference in thickness ($4.7mm$ & $3.0mm$, respectively) and thus were expected to have significant differences in solidification time, cell size (secondary dendrite arm spacing) and porosity.

An aging treatment (T6) was performed according to modified ASTM B661 specifications [10]. Specimens were encapsulated in argon and solution treated at 413 °C for $20h$. Following a water quench, specimens were aged for $50h$ at 413 °C.

Axial fatigue tests were performed using a MTS servo-hydraulic test machine with a FlexTest SE controller and MTS TestSuite control software. All tests were performed in total strain control with a strain ratio of $R(\epsilon_{min}/\epsilon_{max}) = -1$ and a constant frequency of 5 Hz. Specimens were tested in the as-cast and T6 conditions from L1 and L2 at total strain amplitudes of 0.2%, 0.4% and 0.6%. A minimum of four specimens was tested for each location/condition/total strain amplitude. Failure was defined as complete specimen separation or 20% tensile load drop. Tests were performed in laboratory air at 25 °C and according to ASTM E606 [11].

Incremental step tests (IST) had a total strain amplitude of 1.0%, 60 cycles per block, constant strain rate of $0.01sec^{-1}$ and $R = -1$. A total strain amplitude of 1.0% was chosen to prevent failure before a stable state was established. Specimens were tested until complete separation, normally six cycles. One specimen was tested for each location/condition. Tests were performed in laboratory air at 25 °C. An example IST

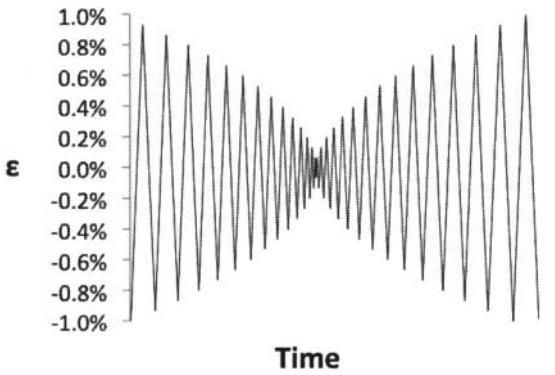

Figure 1: Waveform of a simple IST. In this example there are 30 cycles per block. Strain amplitude changes linearly between cycles.

waveform is shown in Figure 1. An IST allows the determination of the cyclic stress-strain curve from a single specimen [12].

Metallographic preparation involved grinding and polishing to 1 μm particle size. Water was determined to have little effect on the resulting microstructure and was not explicitly avoided during polishing. Samples were ultrasonically cleaned after the final polishing step. The microstructure was examined in the as-polished condition using a Phillips XL30 SEM with a backscatter electron detector. Cell size was measured according to ASTM E112 [13].

Results and Discussion

Microstructure

The microstructure of die-cast AZ91 is shown in Figure 2 and consists primarily of α-Mg. In the as-cast condition, the β phase ($Mg_{17}Al_{12}$) and various intermetallic phases are present in the interdentritic regions. As a result of aging, a eutectic α-Mg and β structure formed along with β precipitates. Intermetallic particles (MnAl) were also present at both conditions. Comparing L1 and L2, a slight difference in average cell size and porosity area fraction was measured (Table I). As expected, L2 had a more refined microstructure with less porosity because of a faster solidification time. L2 also had smaller pores than L1. Heat treatment had negligible effect on porosity. Based on these results, it was expected that L2 would have improved fatigue life because of a smaller cell size and less porosity.

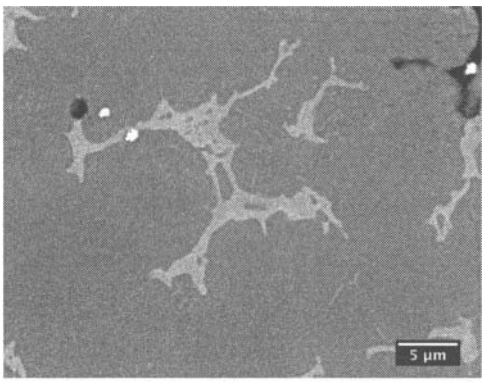

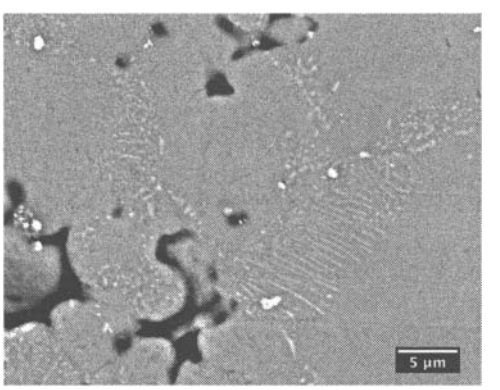

Figure 2: Representative micrographs of as-cast (top) and heat treated (T6) AZ91 (bottom) showing the α-Mg phase (dark) and the β phase ($Mg_{17}Al_{12}$) (light).

Table I: Cell size and porosity for L1 and L2. STDev (Standard Deviation) and STE (Standard Error) are also listed.

	L1	L2
Equivalent Diameter (μm)	4.99	4.17
STDev (μm)	2.26	1.51
STE (μm)	0.05	0.02
Porosity Area Fraction (%)	4.18	1.75

Table II: Low-cycle fatigue test data. N_f^{avg} is the average fatigue-life.

		L1		L2	
	$\Delta\epsilon/2$	As-Cast	T6	As-Cast	T6
N_f^{avg}	0.002	165388	30066	33234	41748
	0.004	6219	5435	5326	4276
	0.006	825	1157	1053	609
STDev	0.002	197977	16944	16092	23144
	0.004	1731	3658	3030	2923
	0.006	557	225	320	382

Axial Fatigue Behavior

The strain-life plot for L1 and L2 in the as-cast and T6 conditions showed a significant amount of scatter at all strain amplitudes (Figure 3). Table II lists the strain-life results in more detail. Results compared favorably with recent literature on die-cast AZ91 [5, 7, 14]. Fatigue-life was an order of magnitude shorter for each strain amplitude when compared with sand cast AZ91 in the T6 condition [8]. Fatigue parameters (Table III) were determined by separating the total strain amplitude into elastic and plastic components and then using Basquin (1) and Coffin-Manson (2) laws, respectively. The fatigue-life relationship based on the total strain can be found by adding equations (1) & (2), resulting in equation (3). For all locations and conditions the fatigue-life data was well described by this approach (Figure 4). Plastic strain was measured from the width of the half-life hysteresis loops at the mean stress. A slightly negative mean stress was observed in most cases due to compression-tension asymmetry (Figure 5).

$$\frac{\Delta\epsilon_e}{2} = \frac{\sigma'_f}{E}(2N_f)^{-b} \tag{1}$$

$$\frac{\Delta\epsilon_p}{2} = \epsilon'_f(2N_f)^{-c} \tag{2}$$

$$\frac{\Delta\epsilon}{2} = \frac{\sigma'_f}{E}(2N_f)^{-b} + \frac{\epsilon'_f}{E}(2N_f)^{-c} \tag{3}$$

where:
$\Delta\epsilon_e$ = true elastic strain range,
$\Delta\epsilon_p$ = true plastic strain range,
$\Delta\epsilon$ = true strain range,
$2N_f$ = reversals to failure,
b = fatigue strength exponent,
c = fatigue ductility exponent,
σ'_f = fatigue strength coefficient,
ϵ'_f = fatigue ductility coefficient, and
E = Youngs modulus (modulus of elasticity).

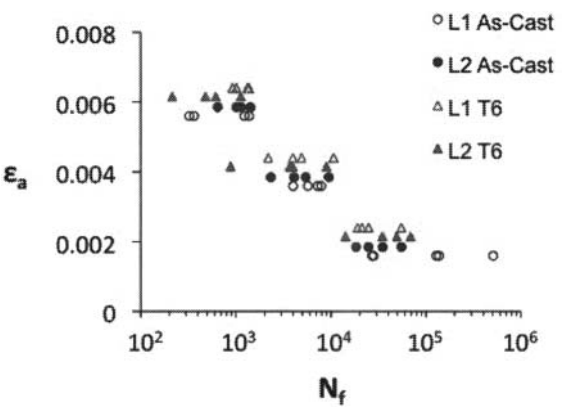

Figure 3: Strain-Life plot for L1 and L2 in the as-cast and T6 conditions. Total strain levels were slightly offset to improve clarity.

Table III: Low-cycle fatigue parameters. N_t is the transition life.

	L1		L2	
	As-Cast	T6	As-Cast	T6
b	0.154	0.243	0.249	0.17
c	0.605	0.771	0.809	0.628
$\sigma'_f(MPa)$	607.5	1323	1386	634.5
ϵ'_f	0.119	0.507	0.785	0.124
N_t	125.4	219.8	324.7	115.8

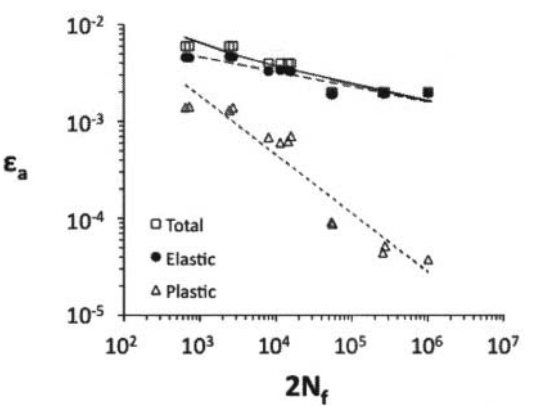

Figure 4: Total, elastic and plastic strain amplitudes vs. number of reversals to failure from L1 in the as-cast condition. Log-log linear regression fits were used to determine the fatigue parameters.

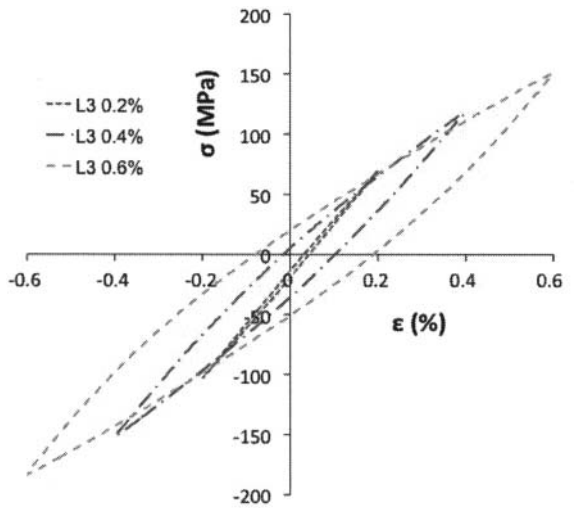

Figure 5: Three representative hysteresis loops from L1 in the as-cast condition corresponding to all three strain amplitudes. Notice the clockwise rotation as the strain amplitude increases and the development of a negative mean stress.

Fractography

Distinct crack growth and fast fracture regions were observed for most failed specimens. Some fracture surfaces experienced severe rubbing during testing and could not be examined. Crack growth regions had a smooth appearance while fast fracture regions showed high contrast regions and cracking around the β phase, similar to fracture surfaces observed from tensile tests [7, 15]. All cracks initiated at either surface or subsurface pores (Figure 6). However, in sand cast AZ91-T6, Goodenberger, et. al. found that cracks initiated primarily at the surface [8]. In samples with shorter fatigue life, fatal cracks initiated from larger pores, similar to results reported by Horstemeyer, et. al. [16]. Pores, present at all locations and conditions, controlled the fatigue life rather than microstructural features.

Fatigue Damage Accumulation

Further examination of crack initiation behavior was done by examining the cross-section on the plane parallel to the stress axis of failed fatigue specimens. Small cracks initiated at pores close to the primary crack for each location/condition (Figure 7). Crack growth appeared to be unaffected by interdentritic and eutectic structures. In some cases, cracks grew parallel to the axis of stress in order to link nearby pores (Figure 8).

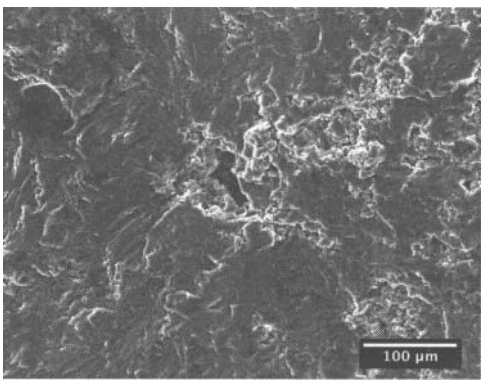

Figure 6: A representative SEM fractograph showing a typical crack initiation pore from L1 in the as-cast condition. This particular specimen had the longest fatigue life (N_f = 506791) and a crack initiation pore size of 72 μm.

There did not appear to be general or wide spread crack initiation and growth away from the fracture plane, indicating the dominant role of a single pore or a cluster of closely spaced pores in damage accumulation.

Cyclic Stress-Strain Behavior

The monotonic and cyclic stress-strain parameters (Table IV) were characterized using two power-law fits, equations (4) & (5), respectively. Methods were similar to those described previously to determine low-cycle fatigue parameters. Comparing monotonic and cyclic loading conditions, the strain-hardening rate is higher in cyclic loading and the yield strength is lower, indicating cyclic softening. Heat treatment had a negligible effect on the strain-hardening rate but did increase the yield strength for both locations under cyclic loading.

$$\frac{\Delta\sigma}{2} = K\left(\frac{\Delta\epsilon_p}{2}\right)^n \tag{4}$$

$$\frac{\Delta\sigma}{2} = K'\left(\frac{\Delta\epsilon_p}{2}\right)^{n'} \tag{5}$$

where:
$\Delta\sigma$ = true stress range,
$\Delta\epsilon_p$ = true plastic strain range,
n = monotonic strain hardening exponent,
n' = cyclic strain hardening exponent,
K = monotonic strength coefficient, and
K' = cyclic strength coefficient.

Table IV: Monotonic(M)/cyclic(C) stress-strain parameters.

	L1				L2			
	As-Cast		T6		As-Cast		T6	
	M	C	M	C	M	C	M	C
n/n'	0.185	0.417	0.246	0.400	0.140	0.481	0.233	0.419
$K/K'(MPa)$	482	2140	737	2153	393	3561	671	2334
$E(GPa)$	43.1	43.9	44.7	44.8	42.0	42.7	44.9	43.7
$Y_s(MPa)$	155	136	160	151	166	138	155	142

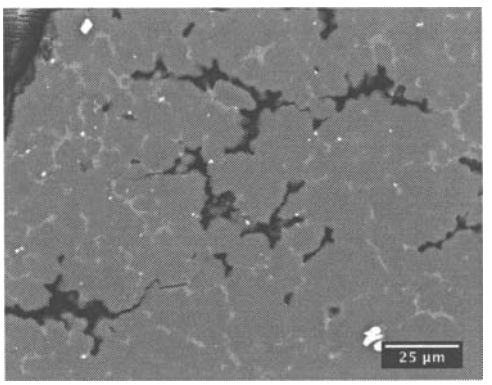

Figure 7: Micrograph from L1 in the as-cast condition showing cracks initiating at pores near the primary crack. Stress axis is parallel to the long direction of the page. Part of the primary crack (fracture surface) can be seen in the upper left corner.

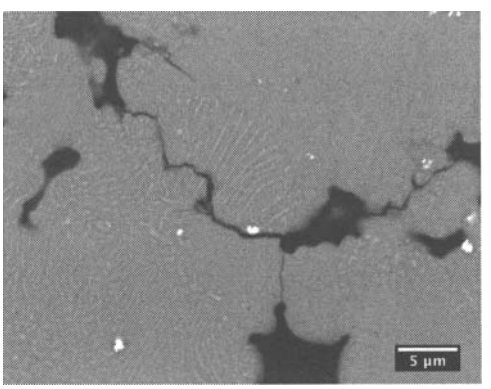

Figure 8: Micrograph from L2 in the T6 condition. A crack in this figure grew parallel to the stress axis in order to link two nearby pores. Stress axis is parallel to the long direction of the page.

Conclusions

1. Fatigue-life was controlled by porosity at both locations/conditions, for all strain amplitudes and was independent of microstructure and heat treatment. In general the larger the initiation pore the shorter the fatigue life.
2. Crack growth from pores was uninhibited by interdentritic and eutectic structures. The crack growth direction was typically perpendicular to the stress axis, however, the driving factor for cracks to link with nearby pores caused some cracks to grow parallel to the stress axis.
3. Cyclic loading caused an increased hardening rate and reduced the yield strength. The cyclic yield strength can be improved with a T6 heat treatment.

Acknowledgments

The authors would like to thank USAMP for funding Project AMD703 and members (specifically Jason Geathers and Garret Huff) of the Fatigue Lab at the University of Michigan for their assistance and guidance.

References

1. E. Aghion and B. Bronfin, "Magnesium Alloys Development towards the 21st Century," *Materials Science Forum*, vol. 350-351, pp. 19–30, 2000.
2. "Magnesium Vision 2020: A North American Automotive Strategic Vision for Magnesium, U.S. Automotive Materials Partnership, (USAMP) U.S. Council for Automotive Research (USCAR)," Sept. 2010. `www.uscar.org`.
3. J. F. King, "Development of magnesium diecasting alloys," in *Magnesium Alloys and their Applications*, pp. 37–47, Werkstoff-Infomationsgesellschaft, 1998.

4. H. R. Mayer, H. Lipowsky, M. Papakyriacou, R. Rösch, A. Stich, and S. E. Stanzl-Tschegg, "Application of ultrasound for fatigue testing of lightweight alloys," *Fatigue Fracture of Engineering Materials and Structures*, vol. 22, pp. 591–599, July 1999.

5. L. J. Chen, J. Shen, W. Wu, F. Li, Y. Wang, and Z. Liu, "Low-Cycle Fatigue Behavior of Magnesium Alloy AZ91," *Materials Science Forum*, vol. 488-489, pp. 725–728, 2005.

6. G. Eisenmeier, B. Holzwarth, H. Hoppel, and H. Mughrabi, "Cyclic deformation and fatigue behaviour of the magnesium alloy AZ91," *Materials Science and Engineering A*, vol. 319-321, pp. 578–582, Dec. 2001.

7. H. El Kadiri, M. Horstemeyer, J. Jordon, and Y. Xue, "Fatigue Crack Growth Mechanisms in High-Pressure Die-Cast Magnesium Alloys," *Metallurgical and Materials Transactions A*, vol. 39, pp. 190–205, Jan. 2008.

8. D. L. Goodenberger and R. I. Stephens, "Fatigue of AZ91E-T6 Cast Magnesium Alloy," *Journal of Engineering Materials and Technology*, vol. 115, no. 4, p. 391, 1993.

9. F. Li, Y. Wang, L. Chen, Z. Liu, and J. Zhou, "Low-cycle fatigue behavior of two magnesium alloys," *Journal of Materials Science*, vol. 40, pp. 1529–1531, Mar. 2005.

10. ASTM B661-06, "Standard practice for heat treatment of magnesium alloys," *ASTM*, 2006.

11. ASTM E606-04, "Standard practice for strain-controlled fatigue testing," *ASTM*, 2005.

12. R. W. Landgraf, J. Morrow, and T. Endo, "Determination of the Cyclic Stress-Strain Curve," *Journal of Materials*, vol. 4, no. 1, pp. 176–188, 1969.

13. ASTM E112-96, "Standard test methods for determining average grain size," *ASTM*, 2006.

14. J. P. Li, G. W. Lorimer, J. D. Robson, and B. Davis, "The Microstructures of As-Cast Mg-Zr and Mg-Mn Alloys," *Materials Science Forum*, vol. 488-489, pp. 329–332, 2005.

15. H. Patel, D. Chen, S. Bhole, and K. Sadayappan, "Microstructure and tensile properties of thixomolded magnesium alloys," *Journal of Alloys and Compounds*, vol. 496, pp. 140–148, Apr. 2010.

16. M. Horstemeyer, "High cycle fatigue of a die cast AZ91E-T4 magnesium alloy," *Acta Materialia*, vol. 52, pp. 1327–1336, Mar. 2004.